Influence of the Madden-Julian Oscillation on upper tropospheric humidity

Fabrizio Sassi,[1] Murry Salby,[2] Hugh C. Pumphrey,[3] and William G. Read[4]

Received 25 September 2001; revised 1 February 2002; accepted 5 February 2002; published 4 December 2002.

[1] Variations of upper tropospheric humidity (UTH) and cold cloud in the tropics reveal coherent changes that propagate eastward from the Indian Ocean into the Pacific. The coherence of UTH is high at periods of 30–90 days along the equator. Near the tropical tropopause, UTH coherence is large over the equator in the Indian Ocean and over the subtropics in the central Pacific. A composite life cycle shows that enhanced UTH in the subtropics coincides with two anticyclonic gyres. They straddle anomalous cold cloud over the equator as it propagates eastward. The enhancement of UTH is consistent with anomalously-cold temperature, which mirrors the anticyclonic gyres. Those temperature anomalies cancel the height anomaly of the gyres overhead. The complex of anomalous UTH, cold cloud, and anticyclonic motion marches eastward across the western Pacific, until reaching the dateline. Anomalous convection over the equator then collapses, along with the subtropical gyres and enhanced UTH accompanying it. *INDEX TERMS:* 3374 Meteorology and Atmospheric Dynamics: Tropical meteorology; 3399 Meteorology and Atmospheric Dynamics: General or miscellaneous; 3319 Meteorology and Atmospheric Dynamics: General circulation; 3314 Meteorology and Atmospheric Dynamics: Convective processes; *KEYWORDS:* Madden-Julian Oscillation, Upper Tropospheric Humidity, Tropical Convection

Citation: Sassi, F., M. L. Salby, H. C. Pumphrey, and W. G. Read, Influence of the Madden-Julian Oscillation on upper tropospheric humidity, *J. Geophys. Res.*, *107*(D23), 4681, doi:10.1029/2001JD001331, 2002.

1. Introduction

[2] The Madden-Julian Oscillation (MJO) is a major feature of low-frequency variability in the tropical troposphere; see *Madden and Julian* [1994] for a review. Operating on intraseasonal time scales, the MJO involves an interaction between large-scale dynamics and convection. Details of that interaction are still under investigation. Nevertheless, it is clear the MJO plays a key role in intraseasonal changes of the tropical atmosphere.

[3] A signature of the MJO is visible in tropical wind and cloud [*Madden and Julian*, 1994, and references therein]. It is also visible in humidity structure, although it is poorly understood near the tropical tropopause [*Clark et al.*, 1998; *Maloney and Hartmann*, 1998; *Sandor et al.*, 1998; *Mote et al.*, 2000]. The energy budget of the tropics is influenced importantly by cloud and humidity, especially at upper levels where they sharply modify outgoing longwave radiation. Consequently, variations of cold cloud and upper tropospheric humidity (UTH) figure importantly in efforts to understand the climate of the tropics.

[4] This study examines the interrelationship of UTH, cloud, and motion on intraseasonal timescales. It employs measurements of water vapor in the upper troposphere and lower stratosphere from the Microwave Limb Sounder (MLS) [*Waters et al.*, 1999]. Those measurements are supported by contemporaneous observations of cold cloud in synoptic Global Cloud Imagery, which provides global coverage with high space-time resolution [*Salby et al.*, 1991]. They are also supported by contemporaneous dynamical structure in reanalyses from the European Centre for Medium-Range Weather Forecasts (ECMWF) [*Gibson et al.*, 1997]. Following a review of the data, section 3 examines the space-time behavior of UTH and cold cloud. It reveals episodes wherein the two propagate eastward coherently. The collective signature of cloud, motion, and UTH is then used to composite a life cycle of the MJO, which is interpreted in section 5 in terms of thermal and humidity structure.

2. Data

[5] MLS operated on board the Upper Atmosphere Research Satellite (UARS). Measurements of water vapor in the upper troposphere and lowermost stratosphere are available from September 1991 through April 1993, although not continuously. This study uses measurements between 2 October 1991 and 28 May 1992 from two separate retrievals: At 215 and 146 hPa, humidity is retrieved from radiances of the 205 GHz channel [*Read et al.*, 1995, 2001]. It provides relative humidity, which defines UTH. The average accuracy of UTH profiles measured over the tropics is estimated to be 34% and 20% RHi at 147 and 215 hPa, respectively [*Read et al.*, 2001]. At 100 hPa and higher levels, water vapor mixing

[1]Atmospheric Systems and Analysis, Westminster, Colorado, USA.
[2]University of Colorado, Boulder, Colorado, USA.
[3]Department of Meteorology, University of Edinburgh, Edinburgh, UK.
[4]Jet Propulsion Laboratory, California Institute of Technology, Pasadena, California, USA.

0148-0227/02/2001JD001331$09.00

ratio is retrieved via the stratospheric algorithm described by *Pumphrey* [1998, 1999]. Those retrievals are mapped synoptically, and subsequently converted to relative humidity using ECMWF temperature. Those measurements are in good agreement with contemporaneous balloon observations of water vapor in the lower stratosphere: They are accurate to 0.5 ppmv near 100 Pa, with even greater accuracy at higher levels.

[6] Each of these retrievals provides observations of water vapor that are asynoptic. They have been mapped synoptically via the method described recently by *Salby and Sassi* [2001]. This method rejects undersampled behavior, which dominates asynoptic observations of convective structure, recovering synoptic behavior that operates coherently on large scales. It reflects the large-scale organization of convective properties. Gaps of a couple of days, which are introduced in the tropics by the UARS yaw maneuver, are bridged during the mapping procedure through low-frequency interpolation [*Sassi and Salby*, 1998]. Once transformed into synoptic behavior, UTH can be analyzed in the same fashion as other field properties.

[7] The instantaneous distribution of cold cloud is provided by synoptic Global Cloud Imagery (GCI). Constructed from 6 satellites simultaneously observing the Earth [*Tanaka et al.*, 1991], the GCI provides synoptic images of 11-μm brightness temperature: every 3 hours, with global coverage, and horizontal resolution of 0.5°. Its global coverage with high spatial and temporal resolution enables the GCI to provide observations of cloud contemporaneous with MLS measurements of UTH.

[8] Supporting those observations is dynamical structure in ECMWF reanalyses. Available four times daily, they provide distributions of temperature and motion nearly contemporaneous with observations of humidity from MLS and cloud from the GCI.

3. Space-Time Behavior

[9] The behavior of UTH is presented in Figure 1, along with contemporaneous cold cloud. Figure 1a is a Hovmöller plot of UTH over the equator at 215 hPa (contoured). Superposed is fractional cover by cloud colder than 230 K (shaded), η_{230}, which corresponds to elevations at and above 215 hPa. Each has been low-pass filtered to zonal wave numbers <4 and periods longer than 30 days.

[10] Cold cloud fraction (shaded) is greatest near the dateline, where time-mean η_{230} is large during this period (The period under consideration coincided with the warm phase of El Niño-Southern Oscillation (ENSO), which displaces convection eastward from the western Pacific). Accompanying time-mean structure are several episodes wherein η_{230} is modulated by eastward propagation. One begins on day 1 (2 October 1991) at 60°E and advances eastward, reaching the dateline around day 50 (21 November 1991). Another begins around day 110 (20 January 1992) at 60°E, reaching the dateline some 50 days later. Around day 180 (30 March 1992), a third begins at 60°E, reaching the dateline around day 200 (1 May 1992). A fourth episode begins at about day 210 (19 April 1992), now at 45°E. Cold cloud continues to advance eastward through the close of the record (28 May 1992).

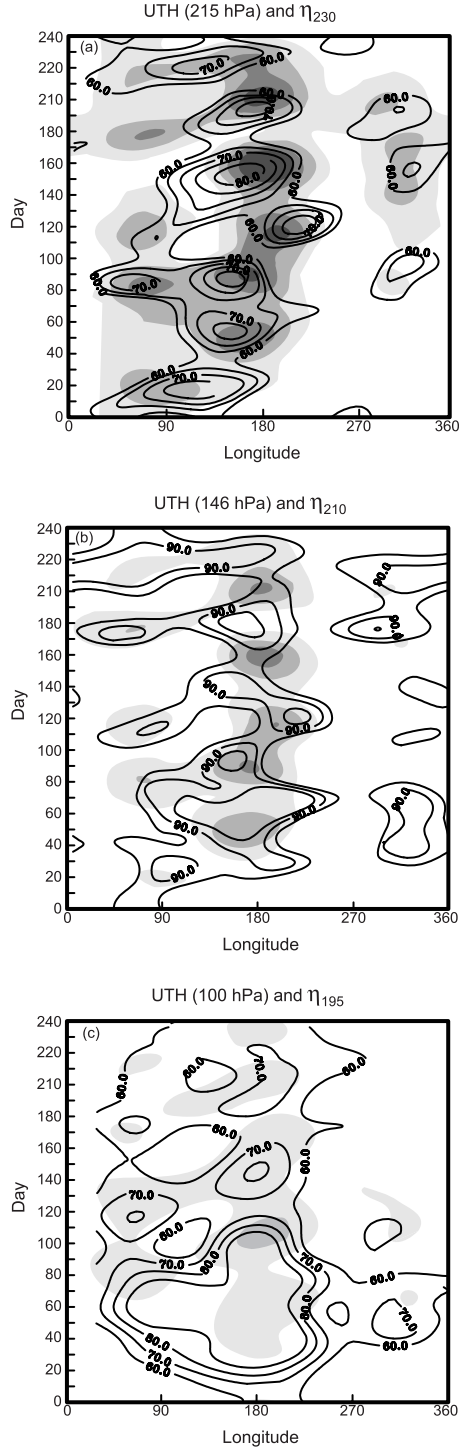

Figure 1. Hovmöller diagrams of relative humidity and cold cloud. (a) Upper tropospheric humidity (UTH) at 215 hPa (contours) and cold cloud fraction η_{230} (shading) at the equator. Contour interval is 5% starting at 60%. Shading levels are 5%, 10%, 15%, and 20%. (b) UTH (contours) at 146 hPa and cold cloud fraction (shading) η_{210} at the equator. Contour interval is 5%, beginning at 85%. Shading levels are 2.5%, 5%, 7.5%. (c) UTH (contours) at 100 hPa and cold cloud fraction (shading) η_{195} at 8S. Contour interval is 10% beginning at 60%. Shading levels are 0.5% and 3%.

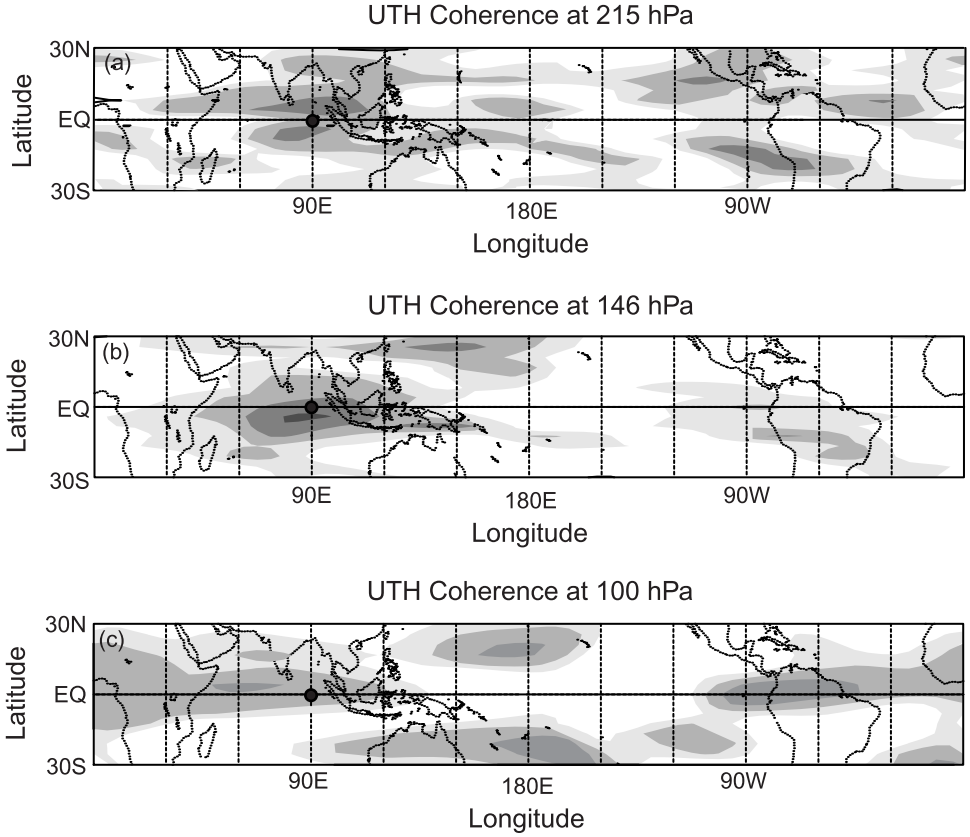

Figure 2. Coherence maps of UTH with cold cloud at 90°E on the equator (location of the reference time series shown by a solid circle). (a) Coherence map of UTH at 215 hPa with η_{230}. (b) UTH at 146 hPa with η_{210}. (c) UTH at 100 hPa with η_{195}. Contour shading is 0.1 starting at 0.5 in all panels. Coherence is shown for band-pass filtered behavior between 30 and 90 days; for each spectral component a spectral average over adjacent 3 frequencies (on either side) was employed.

[11] Resembling the behavior of cold cloud is UTH at the 215 hPa (contoured). Time-mean humidity is also greatest over the central Pacific. Like cold cloud, it experiences several modulations when enhanced UTH advances eastward across the dateline. The Hovmöller plot of UTH reveals eastward propagation between day 1 and day 40, from 60°E to the dateline. Another episode of eastward propagation begins around day 110 and continues through day 150. It leads to a significant enhancement of UTH, which exceeds 80% near the dateline. A third episode begins on day 170. Although weaker than earlier episodes, UTH nonetheless continues eastward through day 200. The final episode begins near day 210, with humidity continuing to advance eastward through the close of the record.

[12] The eastward propagation in Figure 1a reflects variance in η_{230} and UTH at periods of 30–90 days, where spectral power maximizes (not shown). Space-time behavior of cold cloud and UTH at this level operates coherently. Modulations of cold cloud are accompanied by modulations of UTH. The coherence spectrum of the two (not shown) is, in fact, punctuated by a prominent peak at those periods.

[13] Figure 2a illustrates the horizontal structure of anomalous humidity at periods of 30–90 days. It displays the coherence between UTH and η_{230} over the equator at 90°E (solid circle), which serves as a reference time series [*Bath*, 1974]. Plotted is the averaged coherence between periods of 30 and 90 days, at those sites where it is significant at the 95% level. Large coherence straddles the equator over the Indian Ocean and again across the western and central Pacific. It is reduced over the maritime continent but is still statistically significant. Convection there is strongly diurnal, so it is not prominent at periods of 30–90 days: Diurnal behavior can be modulated by 30–90 variability, but that modulation will not be manifested here because satellite data do not resolve it adequately [e.g., *Sassi and Salby*, 1998]. UTH coherence is also large removed from the equator. In fact, it approaches 0.8 in the subtropics of each hemisphere near 120°E and again near South America. Flanking the equator almost symmetrically, these regions of high UTH coherence generally do not coincide with cold cloud, especially in the eastern Pacific where deep convection is inhibited by cold sea surface temperature (SST).

[14] Analogous information is presented for slightly higher levels in Figures 1b and 2b. Figure 1b displays the Hovmöller plot of UTH at 146 hPa, along with fractional cover by cloud colder than 210 K. Apparent is a vertical extension of the three major episodes that characterize cold cloud and UTH at 215 hPa (Figure 1a). Cloud fraction (shaded) is smaller at this level, resulting in somewhat less continuity. On the other hand, UTH (contoured) is greater,

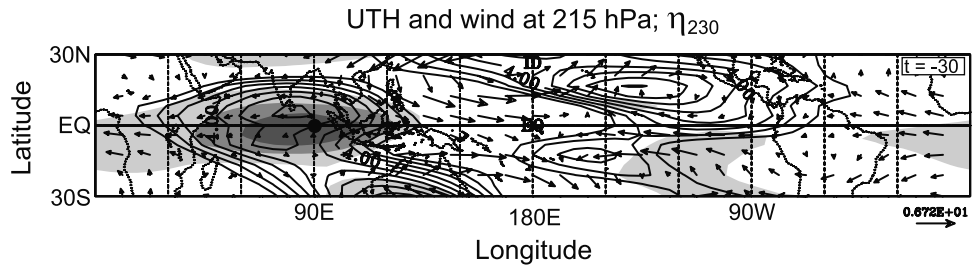

Figure 3. Composite at lag −30 days of UTH (contours) and winds (arrows), both at 215 hPa, and η_{230} (shading). Contour interval is 1%, beginning at +1%. Negative contours are not plotted. Shading levels are 0.5%, 2.0%, and 3.5%. Solid circle at 90°E on the equator shows the position of the clock. The length of the longest vector is 6.7 m s^{-1}.

air at this level approaching saturation. The episodes of eastward propagation seen earlier then lead to major enhancements that drive UTH over 90%.

[15] The horizontal structure of UTH fluctuations is reflected in its coherence with η_{210} over the equator at 90°E, presented in Figure 2b. At this level, coherence is large over the equatorial Indian Ocean, extending eastward south of the equator into the Pacific. Large coherence is also found in the eastern Pacific. Connected to analogous structure at 215 hPa (Figure 2a), this is not a region frequented by cold cloud. Despite its absence, UTH coherence is large to either side of the equator. Its enhancement must involve mechanisms other than vertical transport.

[16] Figure 1c shows the Hovmöller plot of UTH at 100 hPa, near the tropical tropopause. Superposed is fractional cover by cloud colder than 195 K. In each, the signature of eastward propagation along the equator is notably weaker than that visible at lower levels. Nonetheless, UTH (contoured) exhibits an episode of eastward propagation that begins on day 110, reaching the dateline some 30 days later. It coincides with enhanced cold cloud that propagates eastward in similar fashion. An earlier episode is also visible in η_{195}, between days 70 and 100, but the corresponding signature in UTH is obfuscated by persistent cloud cover near the dateline. Another episode begins around day 170, lasting about 40 days, accompanied likewise by eastward propagation of cold cloud.

[17] The corresponding map of UTH coherence is shown in Figure 2c. Coherence with cold cloud at 90°E is strong (approaching 0.8) along the equator over the Indian Ocean. The region of high coherence actually extends eastward from Africa, the Atlantic, and ultimately from South America, where it mirrors coherent structure at lower levels. East of the maritime continent, UTH coherence along the equator decreases sharply. Instead, it becomes large to either side of the equator, in the subtropics of each hemisphere. South of the equator, it even extends into the eastern Pacific, where cold cloud is rare.

4. Composite Life Cycle

[18] The structure of UTH coherence, along with coincident amplification of cold cloud, suggests that humidity is shaped by deep convection and supporting mechanisms. The latter figure prominently near the tropopause, wherein UTH is enhanced even in regions where cold cloud is rare. To articulate this behavior and elucidate the underlying mechanisms, we composite a life cycle of UTH, cold cloud, and horizontal motion, all operating coherently with one another.

[19] The life cycle is composited from the filtered behavior. The filtered record of η_{230} at 90°E on the equator serves as a reference time series, against which we evaluate the phase of fluctuations elsewhere. For a field property ψ, its complex amplitude spectrum $\Psi(m, \sigma)$ is averaged over frequencies σ and wave numbers m within the 30–90 days band. Dates of the filtered behavior are then grouped into a series of phase categories, each category defined by the phase of the complex amplitude calculated from the reference time series (clock).

[20] The composite structure at 215 hPa is presented in Figure 3 for that stage of the life cycle when convection is positioned over the equatorial Indian Ocean. A positive anomaly of UTH (contoured) appears over the Indian Ocean. It mirrors enhanced cold cloud fraction (shaded). This UTH anomaly corresponds to the region of strong coherence in Figure 2a. Accompanying it in the eastern Pacific are two secondary anomalies of enhanced UTH: one north of the equator that extends from the dateline, through the Caribbean, and into the Atlantic, and another south of the equator that extends from the dateline southeastward toward Chile. Those anomalies coincide with regions of strong coherence in Figure 2a. Unlike UTH over the Indian Ocean, however, neither is accompanied by cold cloud. Straddling the equator, they are actually a residual of humidity from previous cycles of the MJO, as will be seen below.

[21] East of enhanced UTH and cold cloud over the Indian Ocean is westerly flow (arrows). It extends across the equatorial Pacific. Moisture transported vertically to this level inside convection [*Sassi et al.*, 2001] is then transported horizontally along the equator. Upon crossing the Pacific, it is carried poleward into each hemisphere.

[22] During subsequent stages of the life cycle (not shown), the anomaly of UTH at 90°E advances eastward across the maritime continent and into the Pacific, until reaching the dateline. Anomalies of opposite sign then form over the Indian Ocean. Corresponding to reduced humidity and cold cloud, they subsequently advance eastward in analogous fashion.

[23] The composite structure at 146 hPa exhibits similar features when anomalous humidity and cold cloud coincide over the equatorial Indian Ocean (not shown). However, after advancing eastward beyond the maritime

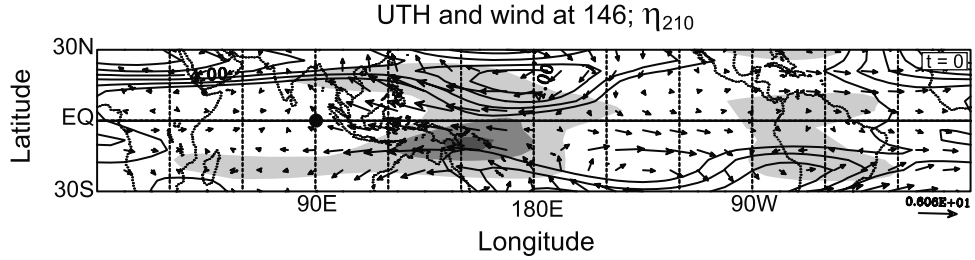

Figure 4. Composite at lag 0 days of UTH (contours) and winds (arrows), both at 146 hPa, and η_{210} (shading). Contour interval is 1%, beginning at +1%. Negative contours are not plotted. Shading levels are 0.1%, 0.8%, and 1.5%. Solid circle at 90°E on the equator shows the position of the clock. The length of the longest vector is 6.1 m s^{-1}.

continent, enhanced humidity and cold cloud separate from one another. Figure 4 presents the composite structure when anomalous cold cloud has invaded the Pacific. At that stage of the life cycle, anomalous humidity is no longer positioned over the equator. Rather, it is enhanced to either side of the equator. Notice that it coincides with anticyclonic motion that also straddles the equator. Immediately to its east are cyclonic anomalies. They coincide with reduced UTH. Cold cloud, on the other hand, remains close to the equator, sandwiched between the two positive anomalies of UTH. It tracks eastward just south of the equator, along the South Pacific Convergence Zone (SPCZ) [cf. *Hendon and Salby*, 1994]. At subsequent stages of the life cycle (not shown), the separated anomalies of cold cloud and humidity continue eastward, until reaching the dateline. Anomalous cold cloud then disappears, leaving a residual of the two humidity anomalies that straddle the equator. Owing to the cyclic nature of the composite life cycle, those anomalies of UTH appear at earlier stages, but farther eastward.

[24] At 100 hPa, near the tropical tropopause, humidity, cold cloud, and motion exhibit even greater symmetry about the equator. Figure 5 plots that structure at the same stage of the life cycle as Figure 4. Humidity at this level (Figure 5a) maximizes off the equator, at this and subsequent stages of the life cycle. Cold cloud over the equator is now clearly sandwiched between two positive anomalies of UTH in the subtropics. They coincide with a pair of anticyclonic gyres that straddle the equator. Notice, however, that those gyres are weaker than counterpart structures immediately below, at 146 hPa. Note also that, at this decaying stage of the life cycle, enhanced cold cloud is found in the region of easterlies, to the west of upper tropospheric divergence [cf. *Hendon and Salby*, 1994].

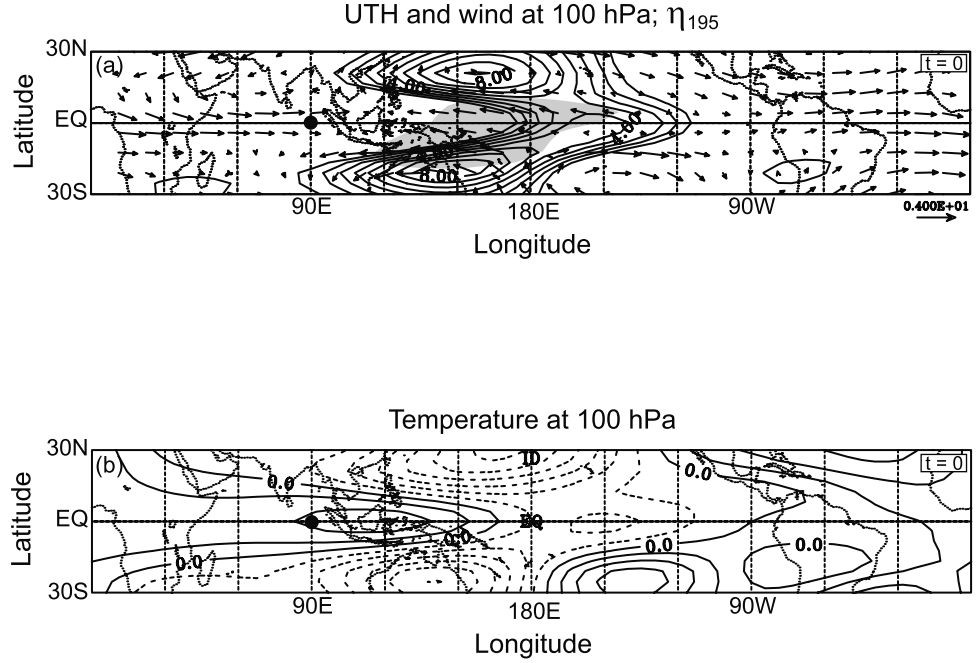

Figure 5. (a) Composite at lag 0 days of UTH (contours) and winds (arrows), both at 100 hPa, and η_{195} (shading). Contour interval is 1%, beginning at +1%. Negative contours are not plotted. Shading levels are 0.1%. The length of the longest vector is 4 m s^{-1}. (b) Composite at lag 0 days of temperature at 100 hPa. Contour interval is 0.25 K. In both panels, solid circle at 90°E on the equator shows the position of the clock.

[25] The gyres and attending anomalies of UTH at this level appear even earlier over the Indian Ocean. The complex of anomalous UTH, cold cloud, and motion then advances eastward, until it reaches the dateline. Anomalous cold cloud, having tracked eastward along the equator, then disappears. Simultaneously, so do the subtropical gyres flanking it and the accompanying anomalies of UTH.

[26] During early stages of the life cycle, anomalous humidity at 100 hPa tracks eastward along the region of strong coherence in the equatorial Indian Ocean (Figure 2c). There, it is collocated with anomalous cold cloud. However, later anomalous humidity coincides with regions of strong coherence off the equator, in the subtropics of the Pacific (Figure 2c). According to the composite structure (Figure 5a), those anomalies of UTH coincide with two anticyclonic gyres that straddle the equator: They flank anomalous convection over the equator, marching eastward with it. The behavior is consistent with the composite life cycle of the MJO, as calculated by *Hendon and Salby* [1994] and *Maloney and Hartmann* [1998].

[27] Coinciding with the subtropical gyres are two cold temperature anomalies (Figure 5b), which likewise straddle the equator. They mirror the positive anomalies of UTH. Anomalous thermal structure accompanying the subtropical gyres is consistent with the anomalies of enhanced UTH. Anomalously cold temperature inside each gyre reduces the saturation mixing ratio r_s, which, in turn, increases relative humidity (equivalent to UTH). Anomalous UTH then tracks eastward with the subtropical gyres. The behavior is associated with vertical deflections of isentropic surfaces as has been reported from radiosonde measurements [*Fujiwara et al.*, 1998].

[28] For the conditions of Figure 5, $T \cong 200$ K, which yields $r_s \cong 16$ ppmv via the Claussius-Clapeyron relation. A temperature anomaly of $\Delta T \cong -1$ K then implies a change of saturation mixing ratio of $\Delta r_s \cong -2$ ppmv. Under cloud-free conditions (Figure 5a) (i.e., in the absence of a localized source of water), this corresponds to no change of mixing ratio r. Together, these changes imply an anomaly of relative humidity of UTH $\cong$7.5%, in reasonable agreement with the observed anomaly of 8.0–9.0%.

5. Conclusions

[29] Near the equator anomalous humidity and cold cloud move eastward jointly from the Indian Ocean, across the maritime continent and into the Pacific. At 215 hPa, fluctuations of UTH operating coherently with convection are strong over the Indian Ocean and the central Pacific. They are smaller over the maritime continent, where convection operates diurnally. The bimodal structure over the Indian Ocean and central Pacific is consistent with anomalous convection associated with the MJO, which amplifies separately in those regions [*Weickman and Khalsa*, 1990; *Zhu and Wang*, 1993; *Salby and Hendon*, 1994]. Enhancements of UTH there reflect vertical transport by deep convection and its humidification of the upper troposphere [*Sassi et al.*, 2001].

[30] A similar relationship appears between anomalous divergence near 200 hPa and MSU precipitation [*Maloney and Hartmann*, 1998]. However, the finer vertical resolution of MLS reveals behavior at upper levels that differs markedly on opposite sides of the maritime continent. To its west, anomalous humidity and cold cloud are collocated, both propagating along the equator. To its east, however, anomalous humidity and cold cloud separate from one another. Cold cloud continues eastward along the equator, but UTH maximizes off the equator in the subtropics of each hemisphere.

[31] Collocated with anticyclonic gyres, anomalies of UTH straddling the equator track eastward with enhanced convection along the equator. They reflect the anomalous circulation of the MJO, which operates sympathetically with convective heating over the equator [*Salby and Hendon*, 1994]. The greatest enhancement of UTH is actually found near the dateline, where temperature is coldest and saturation mixing ratio is most depressed during the period under consideration. Upon reaching the dateline, anomalous convection and the subtropical gyres flanking it disappear, along with attending anomalies of UTH.

[32] Anomalously cold temperature coinciding with the gyres near 100 hPa is "out of phase" with positive anomalous height that defines the anticyclonic circulation. This contrasts with anomalous temperature at lower levels. Tropospheric-mean temperature, measured by MSU channel 2, is ''in phase'' with anomalous height of the subtropical gyres [see *Hendon and Salby*, 1994, Figure 4]. Anomalous temperature operating coherently with the MJO thus reverses near the tropopause, becoming out of phase with anomalous height. This reflects a cancellation of the subtropical gyres at higher levels, noted earlier between 146 and 100 hPa. In fact, their sharply external structure overhead implies a strong negative temperature anomaly. It enhances UTH by decreasing saturation mixing ratio at the upper boundary of the subtropical gyres.

[33] Humidity near the equatorial tropopause is regulated by deep convection, which transports air from the lower troposphere vertically. Episodes of the MJO, by modulating convection, thus modulate radiative energetics that are governed by water vapor absorption. After being introduced at upper levels, that air gradually drifts upward into the stratosphere in ascending motion of the Brewer-Dobson circulation. Episodes of the MJO thus also modulate the humidity of air entering the stratosphere. In addition, the MJO affects horizontal transport. Subtropical gyres, which appear prominently near the tropopause, exchange equatorial air with subtropical air. After leaving the equator, air transported into the upper troposphere by convection moves isentropically. Entrainment into the extratropical circulation can then lead to it being carried along isentropic surfaces into the stratosphere. Modulation of convection by the MJO can thus influence the humidity budget of the stratosphere globally.

[34] **Acknowledgments.** This work was supported by NASA Grant NAG5-6692.

References

Bath, M., Spectral Analysis in Geophysics, Elsevier Sci., New York, 563 pp., 1974.

Clark, H. L., R. S. Harwood, P. W. Mote, and W. G. Read, Variability of water vapor in the tropical upper troposphere as measured by the Microwave Limb Sounder on UARS, *J. Geophys. Res.*, *103*, 31,695–31,707, 1998.

Gibson, J. K., P. Kallberg, S. Uppala, A. Nomura, A. Hernandez, E. Serrano, ERA Description, *ECMWF Re-Analysis Project Rep. Ser. 1*, 74 pp., Shinfield Park, Reading, Mass., 1997.

Fujiwara, M., K. Kita, and T. Ogawa, Stratosphere-troposphere exchange of ozone associated with the equatorial Kelvin wave observed with ozonesondes and rawinsondes, *J. Geophys. Res.*, *103*, 19,173–19,182, 1998.

Hendon, H. H., and M. L. Salby, The life cycle of the Madden-Julian Oscillation, *J. Atmos. Sci.*, *51*, 2225–2237, 1994.

Madden, R., and P. Julian, Observations of the 40–50 day tropical oscillation—A review, *Mon. Weather Rev.*, *121*, 814–837, 1994.

Maloney, E. D., and D. L. Hartmann, Frictional moisture convergence in a composite life cycle of the Madden-Julian Oscillation, *J. Clim.*, *11*, 2387–2403, 1998.

Mote, P. W., H. L. Clark, T. J. Dunkerton, R. S. Harwood, and H. C. Pumphrey, Intraseasonal variations of water vapor in the tropical upper troposphere and tropopause region, *J. Geophys. Res.*, *105*, 17,457–17,470, 2000.

Pumphrey, H. C., Nonlinear retrievals of water vapor from the UARS Microwave Limb Sounder (MLS), *Adv. Space Res.*, *21*(3), 389–392, 1998.

Pumphrey, H. C., Validation of a new prototype water vapor retrieval for the UARS Microwave Limb Sounder, *J. Geophys. Res.*, *104*, 9399–9412, 1999.

Read, W. G., J. Waters, D. A. Flower, L. Froidevaux, R. F. Jarnot, D. L. Hartmann, R. S. Harwood, and R. B. Rood, Upper tropospheric water vapor from UARS MLS, *Bull. Am. Meteorol. Soc.*, *76*, 2381–2389, 1995.

Read, W. G., J. W. Waters, D. L. Wu, E. M. Stone, Z. Shippony, S. Oltmans, D. Kley, H. G. J. Smit, J. L. Mergenthaler, and M. K. Karki, UARS Microwave Limb Sounder upper tropospheric humidity measurement: Method and validation, *J. Geophys. Res.*, *106*, 32,207–32,258, 2001.

Salby, M. L., and H. H. Hendon, Intraseasonal behavior of clouds, temperature, and motion in the Tropics, *J. Atmos. Sci.*, *51*, 2207–2224, 1994.

Salby, M. L., and F. Sassi, Synoptic mapping of convective structure in undersampled satellite observations, *J. Clim.*, *14*, 2281–2295, 2001.

Salby, M. L., H. H. Hendon, K. Woodberry, and K. Tanaka, Analysis of global cloud imagery from multiple satellites, *Bull. Am. Meteorol. Soc.*, *72*, 467–480, 1991.

Sandor, B. J., W. G. Read, J. W. Waters, and K. H. Rosenlof, Seasonal behavior of tropical to midlatitude upper tropospheric water vapor from UARS MLS, *J. Geophys. Res.*, *103*, 25,935–25,947, 1998.

Sassi, F., and M. Salby, Fast Fourier synoptic mapping of UARS data, *J. Geophys. Res.*, *103*, 10,885–19,898, 1998.

Sassi, F., M. Salby, and W. G. Read, Relationship between upper tropospheric humidity and deep convection, *J. Geophys. Res.*, *106*, 17,133–17,146, 2001.

Tanaka, K. H., K. Woodberry, H. H. Hendon, and M. L. Salby, Assimilation of global cloud imagery from multiple satellites, *J. Atmos. Oceanic Technol.*, *8*, 613–626, 1991.

Waters, J. W., et al., The UARS and EOS Microwave Limb Sounder (MLS) experiments, *J. Atmos. Sci.*, *56*, 194–218, 1999.

Weickmann, K. M., and S. J. S. Khalsa, The shift of convection from the Indian Ocean to the western Pacific Ocean during a 30–60 day oscillation, *Mon. Weather Rev.*, *118*, 964–978, 1990.

Zhu, B., and B. Wang, The 30–60 day convection seesaw between the Indian and western Pacific oceans, *J. Atmos. Sci.*, *50*, 184, 1993.

H. C. Pumphrey, Department of Meteorology, University of Edinburgh, Mayfield Road, Edinburgh, EH9 3JZ, UK. (hcp@met.ed.ac.uk)

W. G. Read, California Institute of Technology, Jet Propulsion Laboratory, Mail Stop 183-701, 4800 Oak Grove Drive, Pasadena, CA 91109, USA. (bill@mls.jpl.nasa.gov)

M. Salby, University of Colorado, Boulder, Colorado 80302, USA. (Murry.Salby@Colorado.EDU)

F. Sassi, Atmospheric Systems and Analysis, 1400 West 122nd Avenue, 101, Westminster, CO 80234, USA. (sassi@thunder.asac.org)